Dynamic neuroreceptor positron emission tomography in non-anesthetized rats using point source based motion correction : a feasibility study with [^{11}C]ABP688

Dynamic neuroreceptor positron emission tomography in non-anesthetized rats using point source based motion correction: A feasibility study with [^{11}C]ABP688

Running title: Quantitative [^{11}C]ABP688 PET in awake rats

Tina Kroll[1], Alan Miranda[2], Alexandra Drechsel[1], Simone Beer[1], Markus Lang[3], Alexander Drzezga[1,4,5], Pedro Rosa-Neto[6], Jeroen Verhaeghe[2], David Elmenhorst[1,4*], Andreas Bauer[1*]

[1]*Institute of Neurosciences and Medicine (INM-2), Forschungszentrum Jülich GmbH, Germany*

[2]*Molecular Imaging Center Antwerp, University of Antwerp, Belgium*

[3]*Institute of Neurosciences and Medicine (INM-5), Forschungszentrum Jülich GmbH, Germany*

[4]*Department of Nuclear Medicine, University Hospital Cologne, Germany*

[5]*German Center for Neurodegenerative Diseases (DZNE), Bonn-Cologne, Germany*

[6]*Translational Neuroimaging Laboratory, McGill University Research Centre for Studies in Aging, Alzheimer's Disease Research Unit, Douglas Research Institute, Le Centre intégré universitaire de santé et de services sociaux (CIUSSS) de l'Ouest-de-l'Île-de-Montréal; Department of Neurology and Neurosurgery, Psychiatry and Pharmacology and Therapeutics, McGill University, Montreal, Canada*

* These authors contributed equally to this work.

Corresponding author

Tina Kroll, MD
Institute of Neuroscience and Medicine (INM-2)
Forschungszentrum Jülich GmbH
Wilhelm-Johnen-Straße
52425 Jülich, Germany
Tel: +49 2461 61 96703
Fax: +49 2461 61 2820
E-Mail: t.kroll@fz-juelich.de

Abstract

To prevent motion artifacts in small animal positron emission tomography (PET), animals are routinely scanned under anesthesia or physical restraint. Both may potentially alter metabolism and neurochemistry. This study investigates the feasibility of fully awake acquisition and subsequent absolute quantification of dynamic brain PET data via pharmacokinetic modelling in moving rats using the glutamate 5 receptor radioligand [^{11}C]ABP688 and point source based motion correction.

Five male rats underwent three dynamic [^{11}C]ABP688 PET scans: two test-retest awake PET scans and one scan under anesthesia for comparison. Specific radioligand binding was determined via the simplified reference tissue model (reference: cerebellum) and outcome parameters BP_{ND} and R_1 were evaluated in terms of stability and reproducibility. Test-retest measurements in awake animals gave reliable results with high correlations of BP_{ND} (y=1.08x-0.2, r=0.99, p<0.01) and an acceptable variability (mean over all investigated regions 15.7 ± 2.4%). Regional [^{11}C]ABP688 BP_{ND}s under awake and anesthetized conditions were comparable although in awake scans, absolute radioactive peak uptakes were lower and relative blood flow in terms of R_1 was higher.

Awake small animal PET with absolute quantification of neuroreceptor availability is technically feasible and reproducible thereby providing a suitable alternative whenever effects of anesthesia are undesirable, e.g. in sleep research.

Keywords

awake imaging, [^{11}C]ABP688, point source based motion correction, positron emission tomography, test-retest

Introduction

Positron emission tomography (PET) is a powerful tool to visualize molecular mechanisms in the living organism via various and target-specific radiotracers. In the clinics, PET is mainly used as a diagnostic tool and for monitoring of treatment efficacy. In addition, with an increasing number of suitable radiotracers, this imaging technique gains more and more importance in research offering the opportunity for minimal-invasive analysis of fundamental pathophysiological processes e.g. in the living human brain. Not only in clinical routine and research in humans PET is a powerful tool, but also in preclinical research this technique is now widely applied e.g. in rodents. Especially, generation of animal models mirroring human diseases as well as development of scanners being specifically devoted to rodent imaging fostered preclinical applications of PET during the recent years. However, whereas humans can be told to move as less as possible during the scan session, rodents have to be either restrained or anesthetized to prevent them from moving in the scanner inducing undesirable artifacts to the images. For specific research questions however, narcotics might exert unfavorable effects as general anesthesia putatively interferes with

physiological processes, e.g. sleep-wake regulation (for review see [1]) and glymphatic fluid shifts [2]. Given that PET has the advantage of its applicability in humans and rodents, with regard to translational aspects, anesthesia in preclinical imaging might in general introduce a certain bias as anesthetics influence physiological parameters like body temperature [3], cerebral vascular dynamics [4], and permeability of the blood-brain-barrier [5]. In recent years, it has been shown for several radiotracers that binding to their targets was differentially influenced by varying anesthetics (for review see [6]) minimizing reproducibility and generalization of preclinical results. In baboons, displacement of cerebral [^{18}F]DPA-714 binding to 18kDA translocator protein by the specific antagonist PK11195 occurred under propofol but surprisingly not under isoflurane anesthesia. This further indicates that anesthetics exert important heterogeneous effects on radioligand interactions with their targets including varying target to radioligand affinities [7]. Moreover, Jahreis et al. [8] recently demonstrated that the choice of anesthesia had an important impact on 2-Deoxy-2-[^{18}F]Fluoro-D-Glucose ([^{18}F]FDG) uptake to analyze glucose hypometabolism during epileptogenesis as an early biomarker of disease showing that anesthetics may possibly hamper successful translation to human clinical research.

Consequently, there is a great interest to establish PET imaging in awake animals and during the past decade, a lot of effort was put into the development of methods for preclinical PET imaging in awake rodents to circumvent effects of anesthesia.

Implantation of wireless beta-microprobes [9] or the usage of head mounted mini tomographs [10] for awake imaging is complex and invasive, being moreover restricted to probe implantation in specific target regions without the opportunity to image the whole brain or suffering from limited spatial resolution, respectively. Another option is motion tracking via video systems and attached markers [11, 12] or stereo-optical methods relying on anatomical landmarks [13, 14] for subsequent motion correction of data. Such tracking paradigms however require a complex and expensive set-up and quality of motion correction is highly dependent on exact calibration of the video tracking system and the scanner. Alternatively, fixation of the animals head via specific head holders facilitates imaging of conscious rodents [15, 16] even though immobilization likely causes restraint stress in turn influencing brain physiology putatively resulting in altered outcome parameters of *in vivo* PET studies of awake animals as e.g. shown for [^{18}F]FDG imaging [17]. Altogether, awake PET imaging in small animals should be easily performable without invasive surgery, should be independent of complex and expensive devices, and should allow free movements of animals without any fixation. Recently, a point source based motion tracking method was developed [18] suitable for imaging in awake rats [19] and mice [20] thereby fulfilling all above mentioned criteria. This method is based on ultra-small grains soaked with a positron emitter of a sufficient half-life, which are then attached in different positions onto the animal's head. After list-mode acquisition, data are split into short time frames of 32 ms each, being considered as static, and point

sources are subsequently tracked. The motion information is used in further reconstruction via motion correction algorithms [21].

The current study focuses on the feasibility of fully dynamic quantitative neuroreceptor imaging in awake rats with motion correction via radioactive point sources avoiding any anesthesia during venous radioligand injection and image acquisition. As a pilot [^{11}C]ABP688 specifically binding to the metabotropic glutamate receptor 5 (mGluR5) was used as radiotracer. Animals were repeatedly imaged three times, whereas the first two scans were performed in awake animals to evaluate feasibility of the imaging protocol and to validate test-retest stability of quantification of [^{11}C]ABP688 binding via kinetic modelling of data under awake conditions. The third scan served for comparison of outcome parameters under isoflurane anesthesia.

Material and Methods

Animals & study design

Six adult male Sprague Dawley rats (Charles River Laboratories, Sulzfeld, Germany, mean weight at first imaging session 462 ± 13 g, aged >3 month) were housed in stable groups of two with a 12h lights on – lights off cycle (lights off at 7PM) at ~22°C with food and water provided *ad libitum*. To prevent animals from gaining too much weight in the course of the experiments, calorie-controlled food (Sniff Spezialdiäten GmbH, Soest, Germany) was applied. After arrival, animals were accustomed to the new surroundings for at least three weeks before experiments started and were gradually

habituated to the experimenters and to the cylindrical holder, which was later on used for the awake PET imaging. All animals underwent three imaging sessions of which the first and second was performed under awake condition (test and retest). For comparison, the last scan was conducted under isoflurane anesthesia. Time interval between the test-retest awake scans was 14 ± 1 days (range 12-15 days), whereas time lag between the second awake and comparative third scan under anesthesia was 28 ± 13 days (range 7-41 days). Directly after the last imaging session animals were killed by decapitation under deep isoflurane anesthesia. For one animal, tracer application for the first PET scan failed, leaving data of five animals for analysis. All experiments were conducted in accordance with the German Animal Protection Act and the European Ethics Committee recommendations (Decree 2010/63/CEE) and are reported in compliance with the ARRIVE guidelines. The experiments were approved by regional governmental authorities (Landesamt für Natur, Umwelt und Verbraucherschutz Nordrhein-Westfalen).

PET imaging

For motion tracking of moving animals sodium polyacrylate grains of a diameter of less than 1 mm were first colored with hematoxylin for better visibility (Figure 1A). Subsequently, grains were soaked in [^{18}F]Fluoroethyl-Tyrosine ([^{18}F]FET) and activity of the point sources was measured in a dose calibrator. Target activity was at least 250 kBq, grains which did not reach this activity were again soaked in [^{18}F]FET for a few

seconds. Mean final activity concentration at time of scan start for point sources used as motion markers was 279.3 ± 40.5 kBq (scan 1), 258.4 ± 25.2 kBq (scan 2), and 271.2 ± 7.6 kBq (scan 3). Four of these positron-emitting point sources were attached to the head of the animals in the following positions (Figure 1B): nose (shaved), underneath both ears and right cheek (shaved). Directly afterwards, animals were manually fixed with a towel and a venous catheter (PE10, Becton Dickinson, Sparks, MD, USA) connected to a 30-gauge needle was placed in the tail vein (Figure 1C/D). A cylindrical plastic tube with a diameter of 10 cm and a length of 17.5 cm served as a cage during imaging to prevent animals from moving out of the scanner (Figure 1 D-F). This size of the tube, also being larger than the axial length of the field of view (FOV) of the scanner, was necessary to provide the animals with enough space and to prevent restrainment stress. The tube allowed to place the tail outside (Figure 1 C-E) so that injection of [^{11}C]ABP688 and record of emission scan could be started simultaneously. [^{11}C]ABP688 was produced in-house as described previously [22]. Tracer injection was performed as bolus with a volume of 500 µL constantly applied over 30 s via a syringe pump (model 44, Harvard Apparatus, Holliston, MA, USA). Injected activity of [^{11}C]ABP688 was 28.77 ± 7.05 MBq and 23.13 ± 7.52 MBq for awake test and retest scans and amounted to 23.24 ± 4.68 MBq for scans under anesthesia. During tracer injection, the tail was manually fixed (Figure 1E) and catheters were directly removed after tracer application. During the 70 min emission scan, animals were allowed to freely move within the tube (Figure 1F). As

the length of the tube with 17.5 cm was approximately 5 cm longer than the FOV of the Siemens Inveon PET scanner (Siemens, Knoxville, TN, USA), position of the tube in the FOV was manually adapted when the animal turned around during scanning to ensure that the head of the animal was centered in the FOV most of the scanning time.

For comparative scans under anesthetized condition, isoflurane anesthesia was induced with 5% isoflurane in 2L/min oxygen and maintained at 1.5-2% isoflurane in 1.5 L/min oxygen guided via a respiratory frequency of approximately 50/min. To create comparable conditions, animals were provided with active point sources although animals were immobile. After insertion of tail vein catheters, animals were placed in prone position in the same tube as used for the awake imaging sessions fixed by the nose cone of the anesthesia system. The tube was then placed in the FOV of the scanner and radiotracer injection and image acquisition was done as under awake condition. For general parameters of all imaging sessions see Table 1.

Image reconstruction and analysis

List-mode data of awake scans were motion-corrected as described previously [18]. Subsequently, all data of both awake and anesthetized conditions were reconstructed in a dynamic sequence of 12 x 10s, 3 x 20s, 3 x 30s, 3 x 60s, 3 x 150s, 11 x 300s frames. For awake scans tracking success rates (i.e. percentage of scanning time in which motion tracking was successful) were approximately 81-85% (see Table 1), resulting in some data loss mainly due to animals' brains falling outside of the FOV. Therefore, in some

datasets the number of frames had to be reduced, which was particularly the case for shorter time frames at the beginning of the scan. Data obtained under both conditions were reconstructed, including attenuation correction, as described in [19, 23]. Briefly, for attenuation correction, an initial motion corrected reconstruction served to determine the contour of the animal body to subsequently apply an optimal threshold [24] to the image to separate activity from background. Once the animal body has been delineated, a constant attenuation factor corresponding to soft tissue (0.096 cm^{1}) was assigned to the all body voxels. This image was then applied as attenuation map. Ordered subset list-mode (LM-EM) reconstruction with 16 subsets and 8 iterations was used. In case of awake data motion correction reconstruction was performed. No scatter correction was applied.

All image processing steps were performed with the PMOD software package (version 3.4, PMOD Group, Zurich, Switzerland). First, individual PET images integrated over all time frames were manually co-registered to the rat brain atlas implemented in PMOD. Co-registration included scaling if necessary to ensure that all regions were fully covered by the applied rat brain template. To perform manual co-registration as exact as possible, an image of a computer tomography of an animal of the same species and weight, which was matched to the atlas beforehand, was used to assist co-registration. Transformation matrixes were subsequently applied to dynamic series and co-registration was visually re-checked on all frames. Regional time activity curves were finally generated based on a slightly modified version of the rat brain atlas with the following regions of interest

(ROI) averaged over both hemispheres: Cortex (0.54 mL), cingulate cortex (0.05 mL), caudate-putamen (0.09 mL), thalamus (0.06 mL), hippocampus (0.07 mL) and cerebellar grey matter (0.16 mL).

As blood sampling remains challenging in awake and moving animals during scanning, a reference tissue based approach was chosen to quantify [^{11}C]ABP688 binding [25, 26] under both conditions (awake and anesthesia). Cerebellum served as reference region for modelling of individual datasets with the simplified reference tissue model (SRTM) fitting the three parameters binding potential (BP_{ND}), k_2' (efflux rate of the reference region) and R_1 (representing radioligand delivery in the target region normalized to the reference region) to the TAC by nonlinear regression analysis [27]. Residual weighting was calculated on the basis of measured uptake, radioactive decay correction, and frame length. In short, the BP_{ND} – as a parameter being directly proportional to the maximum number of available receptors – can be described as the ratio of the specifically bound radioligand in the ROI to the non-displaceable portion of the radioligand, which is represented by the activity in the reference-region being void of specific receptors [28], whereas k_2' depicts the efflux rate of the reference region and R_1 represents the regional blood flow in the target region normalized to the reference region.

Parametric BP_{ND} images were generated with non-invasive Logan's graphical analysis [29] with a time point of linearization t^*=10 min.

Statistics

Unless otherwise noted, all values are given as mean ± standard deviation. General parameters of scans performed under both conditions (awake or anesthesia) and for test-retest awake scans were compared using a two-tailed t-test. For comparison of animals' weight, the paired version of the t-test was applied. Normal distribution of BP_{ND} and R_1 as outcome parameters representing mGluR5 availability and relative cerebral blood flow were first checked via Shapiro-Wilk Test. Differences in regional BP_{ND} and R_1 values were than analyzed for different conditions by a mixed model analysis of variance (rmANOVA) with scan session and region treated as within-subject factors. *Post-hoc* paired t-test with Bonferroni correction on the level of investigated regions were subsequently performed to compare regional outcome parameters under different conditions. For the awake status, BP_{ND}s and R_1 values of both test and retest scans were averaged for these comparisons.

Test-retest reproducibility of BP_{ND} and R_1 between both scans under awake condition was evaluated by the relative difference expressed in percentage = (scan 2−scan 1)/scan 1×100%. Analysis of variability was performed by calculating the following parameters: (a) Between subject (BS) and within subject (WS) standard deviation (SD) of the relative difference between scans, (b) Percentage of absolute variability = |scan 2−scan 1|/[(scan 2+scan 1)/2]×100%, (c) Coefficient of variation expressed as percentage (%COV) = SD/mean×100%. The same calculations were performed for comparison of outcome parameters between awake and anesthetized condition.

Relationships between regional outcome parameters were analyzed by the Pearson product-moment correlation coefficient (r) and Bland-Altman Plots [30] were applied to analyze agreement between outcome parameters under different conditions.

All statistical analyses were performed with the SPSS software v.24 (SPSS Inc., Chicago, IL). Orthogonal regression analysis was calculated with MATLAB (version 2019a, Natick, Massachusetts: The MathWorks Inc., 2019).

Results

Besides weight, general scan parameters were not significantly different both for the test-retest scenario under awake conditions nor for the two conditions awake and anesthetized (see Table 1). Figure 2 shows the uptake of [^{11}C]ABP688 for test-retest scans of awake animals (Fig. 2A) and under both awake and anesthetized condition (Fig. 2B). [^{11}C]ABP688 uptake in awake animals was stable and reproducible as shown in Figure 2A. Peak uptake of radioligand occurs under both conditions approximately 30 s after end of injection. Under anesthesia the peak uptake was significantly higher than under awake condition ($p<0.02$). Washout under anesthesia was faster but due to higher peak uptake values, uptake under anesthesia conditions was still slightly elevated during the later time frames of scans in comparison with awake condition (Fig. 2B).

Average parametric images showing mGluR5 availability determined via non-invasive Logan's analysis are depicted for all conditions in Figure 3A, BP_{ND} and R_1 values calculated via kinetic modelling of TACs with SRTM are given in Figure 3B and C.

Highest densities of mGluR5 were observed in caudate-putamen and cingulate cortex under both conditions, awake and anesthetized. Other investigated regions showed moderate mGluR5 availability, whereas regions like hypothalamus and olfactory tract displayed negligible radioligand binding and were therefore not included in further analysis. Comparisons of outcome parameters in terms of BP_{ND} with rmANOVA indicated a significant main effect for region ($F_{(1.76, 7)}$=118.8, p<0.01) but neither for the factor condition (test, retest, and anesthetized, $F_{(1.66, 6.6)}$=0.14, p=0.87) nor for the interaction region × condition ($F_{(2, 7.9)}$=3.3, p=0.09).

Analysis of R_1 with rmANOVA revealed significant differences per region ($F_{(1.5, 6.2)}$=7.4, p=0.026) and a trend significance per condition ($F_{(1.4, 5.6)}$=5.2, p=0.06) whereas the interaction region × condition was not significant ($F_{(1.6, 6.5)}$=2.6, p=0.15). Exploratory paired t-tests revealed no differences in R_1 between the test and retest awake condition in any of the investigated regions. Subsequent reduction of the model to the two conditions awake (by averaging test and retest) and anesthetized indicated significant differences for the terms region ($F_{(1.4, 5.7)}$=13.2, p <0.01), condition ($F_{(1, 4)}$=5.2, p=0.03), and interaction of region × condition ($F_{(2.1, 8.3)}$=8.1, p=0.01). *Post-hoc* analyses via paired t-tests pointed towards discrepancies between awake and anesthetized condition for all regions except for the thalamus of which caudate-putamen and cortex remained significant even after Bonferroni correction on the level of investigated regions (p<0.01, Figure 3C).

BP_{ND} of [^{11}C]ABP688 repeatedly obtained under awake condition revealed high test-retest correlations as shown in Figure 4 A/B. BP_{ND} per animal across all investigated regions scatters closely around the line of identity with high individual correlations coefficients per animal (Figure 4A). Orthogonal regression of mean BP_{ND} values per region illustrates consistency of data (Figure 4B, r=0.99, p<0.01). Bland-Altman plot given in Figure 4C underlines the good agreement without systematic bias. Mean bias averaged over all regions and animals was small with 5.1 ± 17.0% and line of equality is within the confidence interval of the mean difference. Individual regional data points scattered homogenously along both axes showing no relationship of bias and magnitude of BP_{ND}. Moreover, consistent test-retest determination of [^{11}C]ABP688 BP_{ND} was feasible without detecting individual animals as outliers. Detailed values of test-retest stability of [^{11}C]ABP688 BP_{ND} are depicted in Table 2 (upper part). Mean relative difference for all investigated regions was -3.6 ± 3.8% with regional differences ranging from 0.5% (cingulate cortex) to -14.2% (thalamus). Mean variability accounted for 15.7 ± 2.4% (range 13.7% (caudate-putamen) to 18.3% (cortex)).

R_1 values (Figure 4D-F) show equally strong correlations and agreement for test-retest condition as BP_{ND} values except for one outlier in the cingulate cortex (Figure 4D). Detailed parameters for test-retest stability of R_1 values under awake condition are given in Table 2 (upper part).

Regional mGluR5 receptor availability per animal obtained under awake and anesthetized conditions is given as a scatter plot in Figure 5A. Correlations of BP_{ND} values per individual animal across investigated regions were high (Figure 5A). The same was true for correlation of mean values per region ($r=0.97$, $p<0.01$, Figure 5B) and Bland-Altman Plot depicted in Figure 5C illustrates a good to moderate agreement of data obtained under awake and anesthetized condition. No systematic bias could be observed although the slight slope of the regression line points towards a slight tendency of reduced BP_{ND} values in lower to moderate binding regions in awake condition. However, mean absolute differences indicates only a marginal bias of -3.1 ± 21.0% without a systemic influence with regard to magnitude of BP_{ND}. Figure 5 D-F depicts comparisons for R_1 between awake and anesthetized condition. As R_1 values were significantly lower for the anesthetized than for the awake condition, regression line through mean regional values deviated from the line of identity (Figure 5E) and slope of the regression line in the Bland-Altman Plot became negative (Figure 5F). Moreover, R_1 data tended to scatter with individual animals showing disproportionally higher deviations between the two conditions (Figure 5D and F), however, without any regional systematics as different investigated regions were affected. Table 2 (lower part) provides a detailed overview and comparison of regional BP_{ND} and R_1 parameters under awake and anesthetized condition.

Discussion

The present study demonstrates the feasibility of dynamic neuroreceptor PET acquisition under awake condition. We deployed an easy to implement, recently developed, motion tracking via radioactive point sources being independent of external devices [18]. Motion correction can be performed directly on recorded list-mode data in ultra-short and thus static time frames via motion-tracking algorithms based on clearly visible point sources in each time frame [18, 19, 21]. Preparation of point sources is easy, fast and independent of expensive materials. Optimal activities of the point sources used in the current study were empirically defined in validation studies [18, 20] to allow visualization of the point sources in the very short time frames used for motion correction but to avoid excessive scatter or spill-over from the point sources to surrounding tissue. In case of imaging with ^{18}F-labelled radioligands, the same ligand can be used for imaging and preparation of the respective point sources. However, ^{11}C-labelled radioligands, as applied in the current study, might not be suitable for labelling of point sources due to their short half-life and the risk that point sources might not be sufficiently detectable in later time frames of the imaging session. Therefore, for PET studies with ^{11}C-labelled radiotracers as a prerequisite, ^{18}F-Fluorine or any other ^{18}F-labelled radiotracer should be additionally available. As loss of point sources during scanning might result in images not possible to correct for motion artifacts, careful application of a minimum of four point sources onto the animal's head is recommendable. Motion tracking is possible with spatial information of only three or even two sources. In the current study all imaging data could

be corrected for motion as no animal lost more than one point source during awake scanning. However, animals were observed during the whole imaging procedure to prevent them from scratching and thus possible removal of point sources. Thus, one person is solely bound in observation of animals and ideally at least two persons perform measurements. Moreover, for adult rats a tube perfectly fitting into the FOV of a dedicated small animal PET scanner (e.g. axial length of FOV of the Siemens INVEON measures 12.7 cm) is too small to allow animals to move which in turn likely results in restrainment stress potentially influencing imaging results [17].

To reduce the stress level of the animals used in the current study, they were carefully habituated to the tubes used for imaging. At scan days, all animals entered the tubes voluntarily without any pressure by the experimenters. This observation is in line with a recent study showing beneficial effects of tunnel handling in mice [31]. Moreover, the rats did not show any obvious signs of distress, like constant turning or increased breathing frequency, during the imaging sessions. However, when bigger tubes with a length of more than the FOV of the scanner are used as done in the current study, it is essential to take care that the animals' head is consistently in the FOV even when the animal turns around. Otherwise, complete time frames in dynamic data reconstruction will be lost due to insufficient tracking success. This is of special importance for shorter time frames e.g. at early timepoints of dynamic imaging data when injection of radioligands and emission scan are started simultaneously. In the current study, overall tracking success was more

than 80% but especially early, short time frames were missing in certain animals. Nevertheless, these missing time frames did not substantially minimize stability of the outcome parameter BP_{ND} as shown by good to excellent agreement of data gained under anesthesia (with 100% tracking success) and awake condition. Besides, neither general tracking success rate nor percentage of reconstructable frames for the whole acquisition time and time until peak of radiotracer uptake correlated with BP_{ND} in investigated regions.

Image quality and quantitative accuracy of data gained in moving objects with subsequent point source based motion correction was previously determined in phantoms following the procedures of NEMA standards [32]. Even extensive motion of the phantom during the scan sessions, including complete turning of the phantom from back to front, simulating changing positions of a rat's head, only exerts a minor impact on image quality and quantitation of radioactive concentrations in comparison to scans without motion. Especially the visibility of the outline of the body used for μ-map calculation during reconstruction of data, is important for image quality in this context. For a radioligand homogenously distributing throughout the body as used here, outline of the body can be easily determined likely providing a comparable image quality of moving animals as shown in the previous phantom experiments. However, phantom measurements were static and accuracy of especially shorter frames with lower count density during dynamic data acquisition might be inferior than under ideal conditions.

However, even if motion effects on dynamic images might be more pronounced than in static phantom measurements, outcome parameter [^{11}C]ABP688 BP_{ND} as shown here was stable.

[^{11}C]ABP688 binding modelled via the SRTM, which was previously described as the model of choice for quantification of [^{11}C]ABP688 binding under anesthesia [25], exhibits a reliable test-retest stability for rats imaged while being awake albeit test-retest performance was slightly inferior to anesthetized condition [25, 33]. Thus, for test-retest under awake condition mean relative difference and mean variability in BP_{ND} values across all investigated regions was 3.6 ± 3.8% and 15.7 ± 2.4% respectively, whereas previous data under isoflurane anesthesia revealed a relative difference of below 2% and an absolute variability of BP_{ND} of 7.6 ± 5.9%. However, test-retest stability of [^{11}C]ABP688 binding under awake condition is in the same range or even better as for other preclinically used radioligands like e.g. [^{18}F]FDG [34], the dopamine D_2/D_3 antagonist [^{11}C]Raclopride [35], and the adenosine A_1 receptor antagonist 8-cyclopentyl-3-(3-[^{18}F]fluoropropyl)-1-propylxanthine ([^{18}F]CPFPX) [36]. Moreover, awake test-retest stability of [^{11}C]ABP688 BP_{ND} in rats is superior in comparison to non-human primates [37] and humans [38, 39], whereas worse performance in these previous investigation might be at least partly caused by circadian variations of the mGluR5 availability [22] or diurnal alterations in endogenous glutamate levels as subjects were scanned in a test-retest design within one day.

Unlike in recent studies performed with [^{11}C]Flumazenil in awake nonhuman primates [40] and with [^{11}C]Raclopride in awake mice [41], which revealed a trend towards or even significantly higher BP_{ND} values under awake condition with minimal head restraint, [^{11}C]ABP688 BP_{ND} values showed no systematic differences between awake and anesthetized condition in the current study. In comparison to the previous test-retest [^{11}C]ABP688 study [25], it is however striking that determined BP_{ND} values under anesthesia, which served for comparison in the current study, were in general lower than previously determined data. One reason might be the missing scatter correction in the motion correction reconstruction. Although some scatter correction methods for human head motion correction have been developed [42], these approximations do not apply to the case of small animal PET motion correction since the human head motion is largely limited compared to the small animal motion, which can span smaller regions over the entire scanner FOV. For this reason we omitted the scatter correction in the reconstructions. However, in a recent study using a similar motion correction reconstruction in rats, it is stated that rat brain uptake quantification is minimally affected by omission of scatter correction due to the relatively small size of the organ, with a difference of less than 2.5% in quantification comparing reconstructions with and without scatter correction [43]. Hence, different reconstruction algorithms might be more important as reconstruction of the here acquired data with OSEM3D/MAP algorithm instead of LM-EM resulted in approximately 9% higher [^{11}C]ABP688 BP_{ND} values.

Observed differences might, however, also be due to circadian variations of the mGluR5 [22] or due to interindividual variation in mGluR5 availability between samples as [^{11}C]ABP688 BP_{ND} in another study [26] was in the same range as detected here.

Although BP_{ND} values were stable across awake and anesthetized condition, peak uptake of [^{11}C]ABP688 was significantly lower in the awake condition than under isoflurane anesthesia. This might be due to an altered radioligand distribution throughout the body and a faster systemic clearance. However, as we did not gain data of the whole body, this assumption warrants further investigation in future studies. In the context of brain imaging, anesthetics are known to widely influence brain physiology [4] and specifically isoflurane causes vasodilation and increased cerebral blood flow in rats [44] and mice [45], especially in concentrations commonly used for induction and maintenance of anesthesia in rodents [46]. Likely, this effect is at least partly mirrored in [^{11}C]ABP688 time activity curves as activity in early time frames predominantly represents cerebral blood flow even when target specific radioligands are administered [47]. Increased cerebral blood flow in turn could result in increased radioligand supply to the brain under isoflurane anesthesia as recently shown by elevated K_1 values for the synaptic vesicle 2A radiotracer [^{18}F]SynvesT-1 [48]. Besides, putative changes in permeability of the blood-brain barrier [49] and alterations in radiotracer plasma protein binding due to isoflurane administration [50] might further influence radioligand supply and could therefore explain slightly different kinetics of [^{11}C]ABP688 in awake condition. Quantification of radioligand

binding via kinetic models referencing to plasma input function might directly depict these alterations in terms of higher distribution volumes under anesthesia as previously shown for the synaptic vesicle 2A radiotracer [^{18}F]SynvesT-1 [48]. Interestingly, in the current study R_1 values indicate a region-dependent influence of isoflurane on cerebral blood flow. R_1 is the ratio of influx constants of target and reference region whereby the influx constants are the product of radioligand extraction and cerebral blood flow. Previous studies with [^{11}C]PiB and [^{15}O]water in humans showed that R_1 could serve as a proxy for relative cerebral blood flow [51]. In the current study under awake condition R_1 scatters around 1 but decreased under isoflurane anesthesia to 0.7-0.8 in all regions except for the thalamus pointing towards a more pronounced increase of cerebral blood flow under isoflurane anesthesia in the reference region cerebellum than in (cortical) target regions. This observation is in line with region-dependent effects of isoflurane on cerebral blood flow in humans with predominant increases in subcortical and infratentorial regions [52, 53]. In addition, heterogeneous effects of isoflurane throughout the brain were previously observed for the confirmation of the blood-brain barrier as Tétrault et al. were able to show an opening of the BBB by isoflurane specifically in the thalamus after low-dosage isoflurane application in humans [49]. This finding might explain the absent variation of R_1 values between awake and anesthetized condition solely in the thalamus in the current study. However, these phenomena warrant further investigation as some missing time frames especially in the beginning of the acquisition

of awake PET data in the current study as well as missing scatter correction might influence determination of R_1 values.

Noticeable, previous determination of R_1 in rats of the same strain and weight investigated with the same radioligand under isoflurane anesthesia supplied in equal concentration as in the current study resulted in considerably higher R_1 values of approximately 1.3 for cortical and subcortical regions [25]. Reasons for these discrepancies between data both acquired under general anesthesia are unknown but might be at least partly caused by different oxygen flows during narcosis in the two studies. In detail, Elmenhorst et al. used 0.5 L O_2/min whereas in the current study oxygen was applied with a flow of 1.5 L/min. Alterations in oxygenation might in turn also influence cerebral hemodynamics as hypoxia was shown to reduce cerebral blood flow. Interestingly, this reduction was even more pronounced in anesthetized rats [54] indicating that under general anesthesia rodents might be more sensitive towards alterations in oxygen level and already react with changes in cerebral blood flow even when only minor changes in pO_2 occur. These findings further suggest that differing anesthesia protocols even when using the same narcotic might introduce a certain variability to parameters determined in a full kinetic modelling approach.

In conclusion, full quantitative awake small animal neuroreceptor PET imaging is technically feasible and reproducibly performable without any anesthesia as shown here for [^{11}C]ABP688. Although, test-retest reproducibility of data acquired under awake

conditions was found to be slightly inferior in comparison to previous data obtained under anesthesia, longitudinal designs are suitable for [^{11}C]ABP688 imaging studies in awake moving rats to reduce both interindividual noise and animal numbers. Such alternative imaging protocols without any application of anesthetics are of special interest for investigation of physiological effects naturally interfering with anesthesia, like for research in sleep, chronobiology and glymphatic flow. Observed lower [^{11}C]ABP688 uptake and higher R_1 values under awake condition indicated that isoflurane anesthesia alters cerebral hemodynamics, but as [^{11}C]ABP688 binding potential were stable for both conditions, imaging protocols under anesthesia provide valid quantification of mGluR5 availability with [^{11}C]ABP688 PET. To what extent the current results can be transferred to other radioligands should be evaluated in future studies to gain more insights in effects of anesthesia on dynamic acquisition and subsequent full quantitative analysis of preclinical PET data.

Acknowledgement

Nadja Hermes, Sabine Jakobs, Sabina Klein, Angela Oskamp, Sylvia Köhler-Dibowski, and Stephanie Krause are gratefully acknowledged for excellent technical assistance. We thank Nikola Kornadt-Beck and her team for fruitful discussions, animal care taking and valuable support.

Author contribution

TK, AM, DE, and AB designed the study, TK analyzed data being acquired by TK, AM, and AD. ML synthetized the radioligand, whereas AM and JV reconstructed data and developed and optimized motion tracking algorithms. TK wrote the first draft of the manuscript which was revised and edited by AM, DE, SB, ADrz, PRN, JV, and AB. All authors assisted in reviewing the manuscript and approved the final version of this manuscript.

Funding

This project was part of the ERA-NET NEURON project SleepLess supported by BMBF (01EW1808), FWO and FRQS under the frame of Neuron Cofund.

Conflict of interest

The authors, except for those below, declared no potential conflicts of interest with respect to the research, authorship, and/or publication of this article.

Alexander Drzezga: Research support: Siemens Healthineers, Life Molecular Imaging, GE Healthcare, AVID Radiopharmaceuticals, Sofie, Eisai, Novartis/AAA, Ariceum Therapeutics

Speaker Honorary/Advisory Boards: Siemens Healthineers, Sanofi, GE Healthcare, Biogen, Novo Nordisk, Invicro, Novartis/AAA, Bayer Vital

Stock: Siemens Healthineers, Lantheus Holding, Structured therapeutics, ImmunoGen

Patents: Patent for 18F-JK-PSMA- 7 (Patent No.: EP3765097A1; Date of patent: Jan. 20, 2021).

Data Availability Statement

The datasets generated and analyzed during the current study are available from the corresponding author on reasonable request.

Reference List

1. Moody OA, Zhang ER, Vincent KF, et al. The Neural Circuits Underlying General Anesthesia and Sleep. *Anesth Analg* 2021; 132: 1254-1264. 2021/04/16. DOI: 10.1213/ane.0000000000005361.
2. Benveniste H, Heerdt PM, Fontes M, et al. Glymphatic System Function in Relation to Anesthesia and Sleep States. *Anesth Analg* 2019; 128: 747-758. 2019/03/19. DOI: 10.1213/ane.0000000000004069.
3. Kiyatkin EA. The hidden side of drug action: brain temperature changes induced by neuroactive drugs. *Psychopharmacology (Berl)* 2013; 225: 765-780. 2013/01/01. DOI: 10.1007/s00213-012-2957-9.
4. Slupe AM and Kirsch JR. Effects of anesthesia on cerebral blood flow, metabolism, and neuroprotection. *J Cereb Blood Flow Metab* 2018; 38: 2192-2208. 2018/07/17. DOI: 10.1177/0271678x18789273.
5. Noorani B, Chowdhury EA, Alqahtani F, et al. Effects of Volatile Anesthetics versus Ketamine on Blood-Brain Barrier Permeability via Lipid-Mediated Alterations of Endothelial Cell Membranes. *J Pharmacol Exp Ther* 2023; 385: 135-145. 2023/02/25. DOI: 10.1124/jpet.122.001281.
6. Alstrup AK and Smith DF. Anaesthesia for positron emission tomography scanning of animal brains. *Lab Anim* 2013; 47: 12-18. 2013/01/26. DOI: 10.1258/la.2012.011173.
7. Saba W, Goutal S, Kuhnast B, et al. Differential influence of propofol and isoflurane anesthesia in a non-human primate on the brain kinetics and binding of [(18)F]DPA-714, a positron emission tomography imaging marker of glial activation. *Eur J Neurosci* 2015; 42: 1738-1745. 2015/05/13. DOI: 10.1111/ejn.12946.
8. Jahreis I, Bascuñana P, Ross TL, et al. Choice of anesthesia and data analysis method strongly increases sensitivity of 18F-FDG PET imaging during experimental epileptogenesis. *PLoS One* 2021; 16: e0260482. 2021/11/25. DOI: 10.1371/journal.pone.0260482.
9. Märk J, Benoit D, Balasse L, et al. A wireless beta-microprobe based on pixelated silicon for in vivo brain studies in freely moving rats. *Phys Med Biol* 2013; 58: 4483-4500. 2013/06/14. DOI: 10.1088/0031-9155/58/13/4483.
10. Woody C, Dzhordzhadze V, Fontaine R, et al. The RatCAP conscious small animal PET tomograph. In: *Nuclear Science Symposium/Medical Imaging Conference* Rome, ITALY, Oct 16-22 2004, 2004 ieee nuclear science symposium conference record, vols 1-7, pp.2334-2338.
11. Kyme AZ, Angelis GI, Eisenhuth J, et al. Open-field PET: Simultaneous brain functional imaging and behavioural response measurements in freely moving small animals. *Neuroimage* 2019; 188: 92-101. 2018/12/07. DOI: 10.1016/j.neuroimage.2018.11.051.
12. Kyme AZ, Zhou VW, Meikle SR, et al. Optimised motion tracking for positron emission tomography studies of brain function in awake rats. *PLoS One* 2011; 6: e21727. 2011/07/13. DOI: 10.1371/journal.pone.0021727.

13. Kyme A, Se S, Meikle S, et al. Markerless motion tracking of awake animals in positron emission tomography. *IEEE Trans Med Imaging* 2014; 33: 2180-2190. 2014/07/06. DOI: 10.1109/tmi.2014.2332821.
14. Kyme AZ, Aksoy M, Henry DL, et al. Marker-free optical stereo motion tracking for in-bore MRI and PET-MRI application. *Med Phys* 2020; 47: 3321-3331. 2020/04/25. DOI: 10.1002/mp.14199.
15. Khubchandani M, Mallick HN, Jagannathan NR, et al. Stereotaxic assembly and procedures for simultaneous electrophysiological and MRI study of conscious rat. *Magn Reson Med* 2003; 49: 962-967. 2003/04/22. DOI: 10.1002/mrm.10441.
16. Momosaki S, Hatano K, Kawasumi Y, et al. Rat-PET study without anesthesia: anesthetics modify the dopamine D1 receptor binding in rat brain. *Synapse* 2004; 54: 207-213. 2004/10/12. DOI: 10.1002/syn.20083.
17. Sung KK, Jang DP, Lee S, et al. Neural responses in rat brain during acute immobilization stress: a [F-18]FDG micro PET imaging study. *Neuroimage* 2009; 44: 1074-1080. 2008/10/28. DOI: 10.1016/j.neuroimage.2008.09.032.
18. Miranda A, Staelens S, Stroobants S, et al. Fast and Accurate Rat Head Motion Tracking With Point Sources for Awake Brain PET. *IEEE Trans Med Imaging* 2017; 36: 1573-1582. 2017/02/17. DOI: 10.1109/tmi.2017.2667889.
19. Miranda A, Kang MS, Blinder S, et al. PET imaging of freely moving interacting rats. *Neuroimage* 2019; 191: 560-567. 2019/03/05. DOI: 10.1016/j.neuroimage.2019.02.064.
20. Miranda A, Glorie D, Bertoglio D, et al. Awake (18)F-FDG PET Imaging of Memantine-Induced Brain Activation and Test-Retest in Freely Running Mice. *J Nucl Med* 2019; 60: 844-850. 2018/11/18. DOI: 10.2967/jnumed.118.218669.
21. Miranda A, Staelens S, Stroobants S, et al. Motion Dependent and Spatially Variant Resolution Modeling for PET Rigid Motion Correction. *IEEE Trans Med Imaging* 2020; 39: 2518-2530. 2020/02/20. DOI: 10.1109/tmi.2019.2962237.
22. Elmenhorst D, Mertens K, Kroll T, et al. Circadian variation of metabotropic glutamate receptor 5 availability in the rat brain. *J Sleep Res* 2016; 25: 754-761. 2016/07/01. DOI: 10.1111/jsr.12432.
23. Angelis G, Bickell M, Kyme A, et al. Calculated attenuation correction for awake small animal brain PET studies. In: *2013 IEEE Nuclear Science Symposium and Medical Imaging Conference (2013 NSS/MIC)* 27 Oct.-2 Nov. 2013 2013, pp.1-4.
24. Xu X, Xu S, Jin L, et al. Characteristic analysis of Otsu threshold and its applications. *Pattern Recognition Letters* 2011; 32: 956-961. DOI: https://doi.org/10.1016/j.patrec.2011.01.021.
25. Elmenhorst D, Aliaga A, Bauer A, et al. Test-retest stability of cerebral $mGluR_5$ quantification using [^{11}C]ABP688 and positron emission tomography in rats. *Synapse* 2012; 66: 552-560. 2012/02/01. DOI: 10.1002/syn.21542.
26. Elmenhorst D, Minuzzi L, Aliaga A, et al. In vivo and in vitro validation of reference tissue models for the mGluR(5) ligand [(11)C]ABP688. *J Cereb Blood Flow Metab* 2010; 30: 1538-1549. 2010/06/10. DOI: 10.1038/jcbfm.2010.65.

27. Lammertsma AA and Hume SP. Simplified reference tissue model for PET receptor studies. *Neuroimage* 1996; 4: 153-158. 1996/12/01. DOI: 10.1006/nimg.1996.0066.
28. Innis RB, Cunningham VJ, Delforge J, et al. Consensus nomenclature for in vivo imaging of reversibly binding radioligands. *J Cereb Blood Flow Metab* 2007; 27: 1533-1539. 2007/05/24. DOI: 10.1038/sj.jcbfm.9600493.
29. Logan J, Fowler JS, Volkow ND, et al. Distribution volume ratios without blood sampling from graphical analysis of PET data. *J Cereb Blood Flow Metab* 1996; 16: 834-840. 1996/09/01. DOI: 10.1097/00004647-199609000-00008.
30. Bland JM and Altman DG. Agreement between methods of measurement with multiple observations per individual. *J Biopharm Stat* 2007; 17: 571-582. 2007/07/07. DOI: 10.1080/10543400701329422.
31. Gouveia K and Hurst JL. Improving the practicality of using non-aversive handling methods to reduce background stress and anxiety in laboratory mice. *Sci Rep* 2019; 9: 20305. 2020/01/01. DOI: 10.1038/s41598-019-56860-7.
32. Beer S, Miranda A, Elmenhorst D, et al. Image Quality assessment for Awake Animal Brain PET. *IEEE Nuclear Science Symposium and Medical Imaging Conference (NSS/MIC)*. Manchester, UK: IEEE, 2019, p. 1-3.
33. Wyckhuys T, Verhaeghe J, Wyffels L, et al. N-acetylcysteine- and MK-801-induced changes in glutamate levels do not affect in vivo binding of metabotropic glutamate 5 receptor radioligand 11C-ABP688 in rat brain. *J Nucl Med* 2013; 54: 1954-1961. 2013/09/21. DOI: 10.2967/jnumed.113.121608.
34. Sijbesma JWA, van Waarde A, Vállez García D, et al. Test-Retest Stability of Cerebral 2-Deoxy-2-[(18)F]Fluoro-D-Glucose ([(18)F]FDG) Positron Emission Tomography (PET) in Male and Female Rats. *Mol Imaging Biol* 2019; 21: 240-248. 2018/07/11. DOI: 10.1007/s11307-018-1245-4.
35. Alexoff DL, Vaska P, Marsteller D, et al. Reproducibility of 11C-raclopride binding in the rat brain measured with the microPET R4: effects of scatter correction and tracer specific activity. *J Nucl Med* 2003; 44: 815-822. 2003/05/07.
36. Kroll T, Elmenhorst D, Weisshaupt A, et al. Reproducibility of non-invasive a1 adenosine receptor quantification in the rat brain using [(18)F]CPFPX and positron emission tomography. *Mol Imaging Biol* 2014; 16: 699-709. 2014/03/07. DOI: 10.1007/s11307-014-0729-0.
37. DeLorenzo C, Milak MS, Brennan KG, et al. In vivo positron emission tomography imaging with [^{11}C]ABP688: binding variability and specificity for the metabotropic glutamate receptor subtype 5 in baboons. *Eur J Nucl Med Mol Imaging* 2011; 38: 1083-1094. 2011/02/01. DOI: 10.1007/s00259-010-1723-7.
38. DeLorenzo C, Gallezot JD, Gardus J, et al. In vivo variation in same-day estimates of metabotropic glutamate receptor subtype 5 binding using [(11)C]ABP688 and [(18)F]FPEB. *J Cereb Blood Flow Metab* 2017; 37: 2716-2727. 2016/10/16. DOI: 10.1177/0271678x16673646.

39. DeLorenzo C, Kumar JS, Mann JJ, et al. In vivo variation in metabotropic glutamate receptor subtype 5 binding using positron emission tomography and [11C]ABP688. *J Cereb Blood Flow Metab* 2011; 31: 2169-2180. 2011/07/28. DOI: 10.1038/jcbfm.2011.105.
40. Sandiego CM, Jin X, Mulnix T, et al. Awake nonhuman primate brain PET imaging with minimal head restraint: evaluation of GABAA-benzodiazepine binding with 11C-flumazenil in awake and anesthetized animals. *J Nucl Med* 2013; 54: 1962-1968. 2013/10/12. DOI: 10.2967/jnumed.113.122077.
41. Takuwa H, Maeda J, Ikoma Y, et al. [(11)C]Raclopride binding in the striatum of minimally restrained and free-walking awake mice in a positron emission tomography study. *Synapse* 2015; 69: 600-606. 2015/09/12. DOI: 10.1002/syn.21864.
42. Rahmim A, Dinelle K, Cheng JC, et al. Accurate event-driven motion compensation in high-resolution PET incorporating scattered and random events. *IEEE Trans Med Imaging* 2008; 27: 1018-1033. 2008/08/02. DOI: 10.1109/tmi.2008.917248.
43. Spangler-Bickell MG, de Laat B, Fulton R, et al. The effect of isoflurane on (18)F-FDG uptake in the rat brain: a fully conscious dynamic PET study using motion compensation. *EJNMMI Res* 2016; 6: 86. 2016/11/27. DOI: 10.1186/s13550-016-0242-3.
44. Suzuki C, Kosugi M and Magata Y. Conscious rat PET imaging with soft immobilization for quantitation of brain functions: comprehensive assessment of anesthesia effects on cerebral blood flow and metabolism. *EJNMMI Res* 2021; 11: 46. 2021/05/09. DOI: 10.1186/s13550-021-00787-6.
45. Rakymzhan A, Li Y, Tang P, et al. Differences in cerebral blood vasculature and flow in awake and anesthetized mouse cortex revealed by quantitative optical coherence tomography angiography. *J Neurosci Methods* 2021; 353: 109094. 2021/02/08. DOI: 10.1016/j.jneumeth.2021.109094.
46. Munting LP, Derieppe MPP, Suidgeest E, et al. Influence of different isoflurane anesthesia protocols on murine cerebral hemodynamics measured with pseudo-continuous arterial spin labeling. *NMR Biomed* 2019; 32: e4105. 2019/06/07. DOI: 10.1002/nbm.4105.
47. Hammes J, Leuwer I, Bischof GN, et al. Multimodal correlation of dynamic [(18)F]-AV-1451 perfusion PET and neuronal hypometabolism in [(18)F]-FDG PET. *Eur J Nucl Med Mol Imaging* 2017; 44: 2249-2256. 2017/10/14. DOI: 10.1007/s00259-017-3840-z.
48. Miranda A, Bertoglio D, De Weerdt C, et al. Isoflurane and ketamine-xylazine modify pharmacokinetics of [(18)F]SynVesT-1 in the mouse brain. *J Cereb Blood Flow Metab* 2023: 271678x231173185. 2023/04/28. DOI: 10.1177/0271678x231173185.
49. Tétrault S, Chever O, Sik A, et al. Opening of the blood-brain barrier during isoflurane anaesthesia. *Eur J Neurosci* 2008; 28: 1330-1341. 2008/11/01. DOI: 10.1111/j.1460-9568.2008.06443.x.
50. Dale O and Jenssen U. Interaction of isoflurane with the binding of drugs to proteins in serum and liver cell cytosol. An in vitro study. *Br J Anaesth* 1986; 58: 1022-1026. 1986/09/01. DOI: 10.1093/bja/58.9.1022.
51. Chen YJ, Rosario BL, Mowrey W, et al. PiB Relative Delivery (R1) as a Proxy of Relative Cerebral Blood Flow: Quantitative Evaluation Using Single Session ¹⁵O-Water

and ^{11}C-PiB PET. *Journal of Nuclear Medicine* 2015: jnumed.114.152405. DOI: 10.2967/jnumed.114.152405.
52. Lorenz IH, Kolbitsch C, Hörmann C, et al. Influence of equianaesthetic concentrations of nitrous oxide and isoflurane on regional cerebral blood flow, regional cerebral blood volume, and regional mean transit time in human volunteers. *Br J Anaesth* 2001; 87: 691-698. 2002/03/07. DOI: 10.1093/bja/87.5.691.
53. Reinstrup P, Ryding E, Algotsson L, et al. Distribution of cerebral blood flow during anesthesia with isoflurane or halothane in humans. *Anesthesiology* 1995; 82: 359-366. 1995/02/01. DOI: 10.1097/00000542-199502000-00006.
54. Duong TQ. Cerebral blood flow and BOLD fMRI responses to hypoxia in awake and anesthetized rats. *Brain Res* 2007; 1135: 186-194. 2007/01/03. DOI: 10.1016/j.brainres.2006.11.097.

Table 1: Overview of general parameters of all three imaging sessions

Parameter	Test awake	Retest awake	(paired) t-test
	Mean ± SD		p-value
Weight (g)	462 ± 13	508 ± 19	**0.002**
Start time of emmision scan (hh:mm)	11:20 ± 0:18	11:25 ± 0:18	0.658
Injected dose (MBq)	28.77 ± 7.05	23.13 ± 7.52	0.256
Specific activity (GBq/µmol)	163.98 ± 77.51	152.00 ± 38.79	0.765
Injected amount of radiotracer (nmol)	0.25 ± 0.17	0.20 ± 0.05	0.483
Tracking success rate (%)	84.81 ± 2.52	81.25 ± 2.52	0.142
Travelled distance (m)	30.12 ± 7.99	27.35 ± 4.76	0.523
Mean speed (cm/s)	0.72 ± 0.19	0.65 ± 0.11	0.521

	Awake*	Anesthesia	(paired) t-test
	Mean ± SD		p-value
Weight (g)	485 ± 15	579 ± 51	**0.010**
Start time of emmision scan (hh:mm)	11:22 ± 0:18	11:58 ± 1:42	0.462
Injected dose (MBq)	25.95 ± 7.15	23.24 ± 4.68	0.498
Specific activity (GBq/µmol)	157.99 ± 48.36	203.87 ± 43.57	0.154
Injected amount of radiotracer (nmol)	0.22 ± 0.09	0.13 ± 0.05	0.092

*mean of both scans under awake condition, n=5, significant differences between scan sessions were marked in bold;
SD, standard deviation

Table 2: Test-retest stability of awake [^{11}C]ABP688 imaging (upper part) and overview of outcome parameters under different conditions (awake and anesthetized, lower part): binding potential (BP_{ND}) and relative blood flow (R_1)

		Test awake	Retest awake	% rel Diff.	% Variability	BSSD	WSSD	Correlation
Parameter	Region	Mean ± SD		Mean ± SD		(%COV)		Pearson *r*
BP_{ND}	Cortex	1.46 ± 0.29	1.50 ± 0.35	4.05 ± 20.99	18.28 ± 4.68	0.30 (21%)	0.20 (13%)	0.49
	Cing. Cortex	2.02 ± 0.39	2.01 ± 0.45	0.49 ± 18.44	15.07 ± 8.19	0.40 (20%)	0.22 (11%)	0.55
	Hippocampus	1.61 ± 0.31	1.47 ± 0.18	-7.13 ± 15.54	14.21 ± 10.40	0.25 (16%)	0.15 (10%)	0.62
	CaudatePutamen	2.28 ± 0.39	2.23 ± 0.42	-1.46 ± 15.60	13.69 ± 6.33	0.38 (17%)	0.22 (10%)	0.56
	Thalamus	1.11 ± 0.19	0.94 ± 0.09	-14.17 ± 10.77	16.98 ± 9.83	0.17 (16%)	0.13 (13%)	0.79
R_1	Cortex	0.94 ± 0.11	0.92 ± 0.11	-1.54 ± 12.30	9.23 ± 7.90	0.11 (11%)	0.06 (6%)	0.44
	Cing. Cortex	1.03 ± 0.06	0.88 ± 0.40	-15.04 ± 38.40	35.29 ± 53.54	0.28 (29%)	0.18 (19%)	0.41
	Hippocampus	0.95 ± 0.12	0.94 ± 0.15	-0.63 ± 19.34	14.51 ± 8.91	0.13 (14%)	0.09 (10%)	0.24
	CaudatePutamen	1.05 ± 0.09	1.01 ± 0.10	-2.35 ± 16.07	11.89 ± 9.26	0.09 (9%)	0.09 (8%)	-0.39
	Thalamus	1.04 ± 0.16	1.10 ± 0.09	7.39 ± 12.59	8.50 ± 9.47	0.13 (12%)	0.06 (6%)	0.72
		Awake*	Anesthesia	% rel Diff.	% Variability	BSSD	WSSD	Correlation
		Mean ± SD		Mean ± SD		(%COV)		Pearson *r*
BP_{ND}	Cortex	1.48 ± 0.28	1.45 ± 0.23	1.11 ± 25.16	18.52 ± 14.00	0.24 (16%)	0.18 (12%)	0.11
	Cing. Cortex	2.01 ± 0.37	1.91 ± 0.27	-2.73 ± 21.01	16.56 ± 12.20	0.31 (16%)	0.22 (11%)	0.24
	Hippocampus	1.54 ± 0.22	1.77 ± 0.26	17.38 ± 25.79	18.79 ± 15.98	0.26 (16%)	0.22 (13%)	-0.002
	CaudatePutamen	2.26 ± 0.36	2.25 ± 0.20	2.51 ± 21.92	14.46 ± 13.35	0.27 (12%)	0.22 (10%)	-0.26
	Thalamus	1.02 ± 0.14	1.09 ± 0.17	9.37 ± 25.81	16.40 ± 14.46	0.15 (14%)	0.12 (12%)	-0.18
R_1	Cortex	0.93 ± 0.09	0.70 ± 0.12	-25.17 ± 7.46	29.12 ± 9.89	0.16 (20%)	0.16 (20%)	0.84
	Cing. Cortex	0.95 ± 0.21	0.74 ± 0.17	-20.87 ± 16.07	24.92 ± 19.66	0.21 (25%)	0.15 (18%)	0.66
	Hippocampus	0.94 ± 0.11	0.79 ± 0.09	-15.72 ± 11.74	18.29 ± 12.77	0.12 (14%)	0.11 (13%)	0.37
	CaudatePutamen	1.03 ± 0.05	0.76 ± 0.13	-26.24 ± 11.91	31.09 ± 16.11	0.17 (19%)	0.19 (21%)	0.37
	Thalamus	1.07 ± 0.12	1.06 ± 0.14	0.20 ± 19.80	15.05 ± 10.27	0.12 (11%)	0.11 (10%)	-0.32

*mean of both scans under awake condition, all data were modelled with the simplified reference tissue model, n=5,
BSSD, between subject standard deviation; cing., cingulate; COV, coefficient of variation; rel, relative; diff, difference;
WSSD, within subject standard deviation

Titles and legends to figures

Figure 1: Preparation of flourine-18 soaked point sources (A/B), radioligand injection (C-E) and awake imaging procedure on a Siemens Inveon small animal PET scanner (F).

Figure 2: Tissue time activity curves (TACs) given for selected regions. A) Test-retest comparison of TACs obtained with repeated PET measurements in awake animals. B) TACs for anesthetized and awake condition. For awake condition, the average of both awake scans is shown. Cerebellar TAC was used as reference for subsequent quantification of mGluR5 availability. Mean ± standard error of the mean, n=5. SUV, standardized uptake value (normalized to injected dose and bodyweight)

Figure 3: Quantification of [^{11}C]ABP688 binding (in terms of binding potential (BP_{ND})) and relative regional radioligand delivery (in terms of R_1) under awake and anesthetized condition. A) Parametric images (non-invasive Logan's graphical analysis) of [^{11}C]ABP688 BP_{ND} shown for test and retest under awake condition (upper and middle row) and under isoflurane anesthesia (lower row). Coronal (left), sagittal (middle) and transversal (right) planes are depicted. B) Quantification of BP_{ND} under awake and anesthetized condition via kinetic modelling of data with the simplified reference tissue model (SRTM) with cerebellum as reference region. C) R_1 values modelled with the SRTM for the different conditions and regions. Mean ± standard deviation, n=5, *p<0.05,

**p<0.01 (significance level after Bonferroni correction on the level of investigated regions), for statistical analysis awake data of test and retest were averaged and compared against the anesthetized condition, test and retest data under awake condition did not significantly differ in any of the investigated regions.

Figure 4: Test-Retest stability of [^{11}C]ABP688 binding (in terms of binding potential (BP_{ND})) and relative regional radioligand delivery (in terms of R_1) modelled with the simplified reference tissue model under awake condition. R_1 value of the cingulate cortex in one animal were classified as outlier (see D), data of this animal were omitted in E and F. A/D) Scatter plots of BP_{ND} (A) and R_1 (D) for all investigated regions and animals, individual animals are depicted in different colors, B/E) Correlation of mean regional BP_{ND} (B) and R_1 (E) values. Dotted lines depict lines of identity, solid lines represent orthogonal fits of data (per animal in A) with parameters of regression analysis given in the graphs. C/F) Bland-Altman Plots of BP_{ND} (C) and R_1 (F) values across all investigated regions and animals including mean bias of data (solid horizontal grey line), upper and lower limits of agreement (dashed horizontal lines) with 95% confidence intervals (dotted horizontal lines) and linear regression analysis (solid black lines and parameters given in the upper right of the graphs). n=5, mean ± standard deviation (B/E); cing, cingulate.

Figure 5: Comparison of [^{11}C]ABP688 binding (in terms of binding potential (BP_{ND})) and relative regional radioligand delivery (in terms of R_1) modelled with the simplified reference tissue model under awake and anesthetized condition. For the awake condition outcome parameters of test and retest scans were averaged. A/D) Scatter plots of BP_{ND} (A) and R_1 (D) for all investigated regions and animals, individual animals are depicted in different colors, B/E) Correlation of mean regional BP_{ND} (B) and R_1 (E) values. Dotted lines depict lines of identity, solid lines represent orthogonal fits of data (per animal in A) with parameters of regression analysis given in the graphs. C/F) Bland-Altman Plots of BP_{ND} (C) and R_1 (F) values across all investigated regions and animals including mean bias of data (solid horizontal grey line), upper and lower limits of agreement (dashed horizontal lines) with 95% confidence intervals (dotted horizontal lines) and linear regression analysis (solid black lines and parameters given in the upper right of the graphs). n=5, mean ± standard deviation (B/E); cing, cingulate.

Figure 1

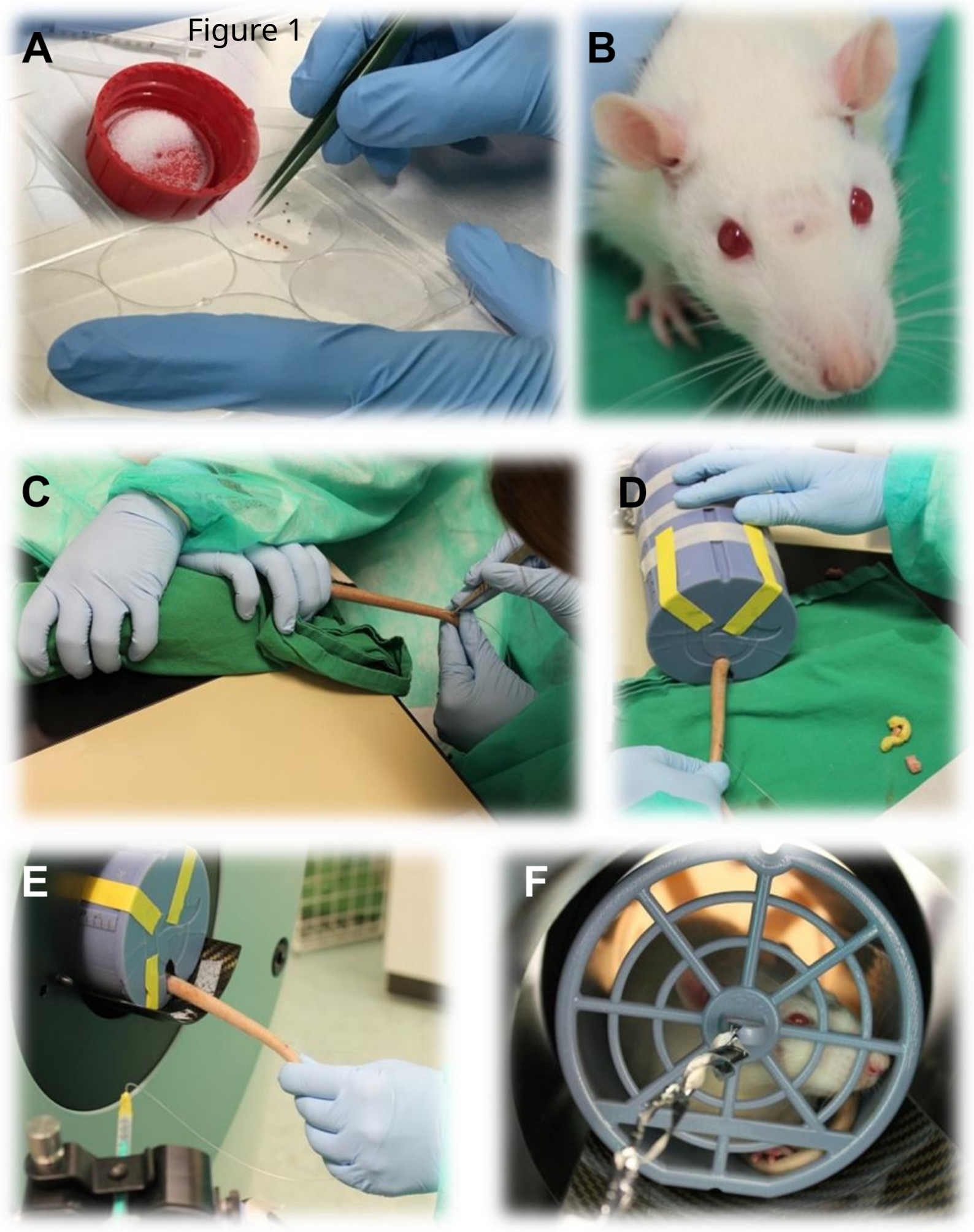

Figure 2

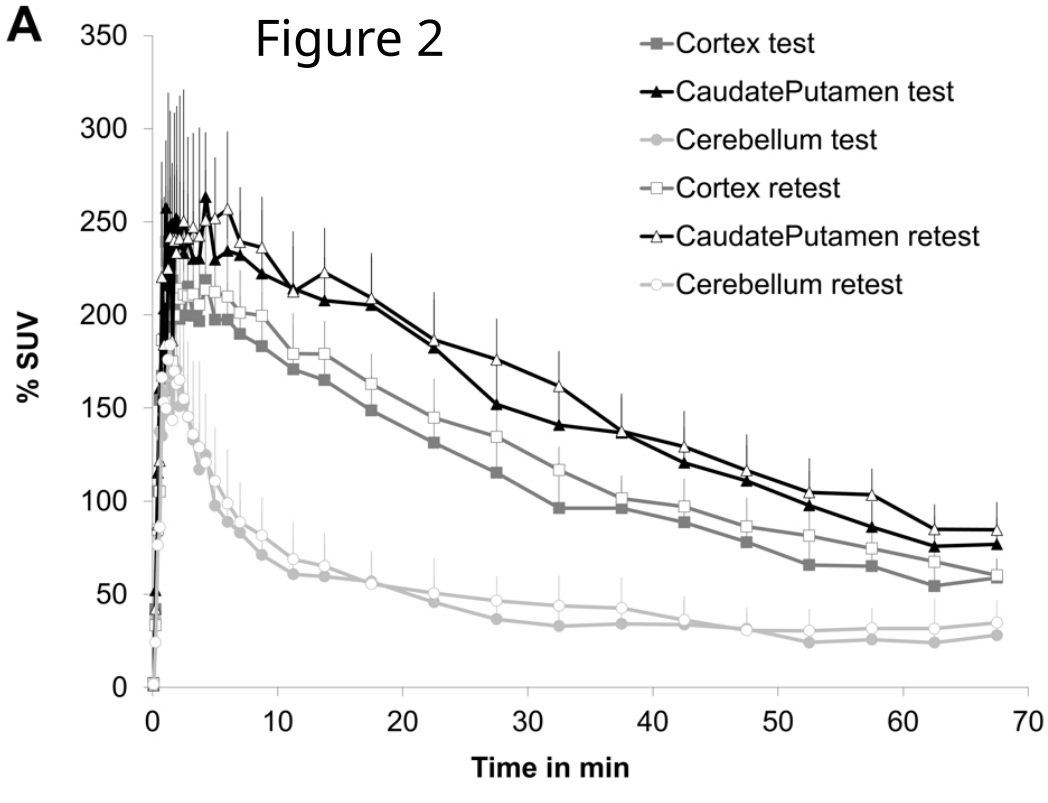
A
Cortex test
CaudatePutamen test
Cerebellum test
Cortex retest
CaudatePutamen retest
Cerebellum retest
% SUV
Time in min
0
50
100
150
200
250
300
350
0
10
20
30
40
50
60
70

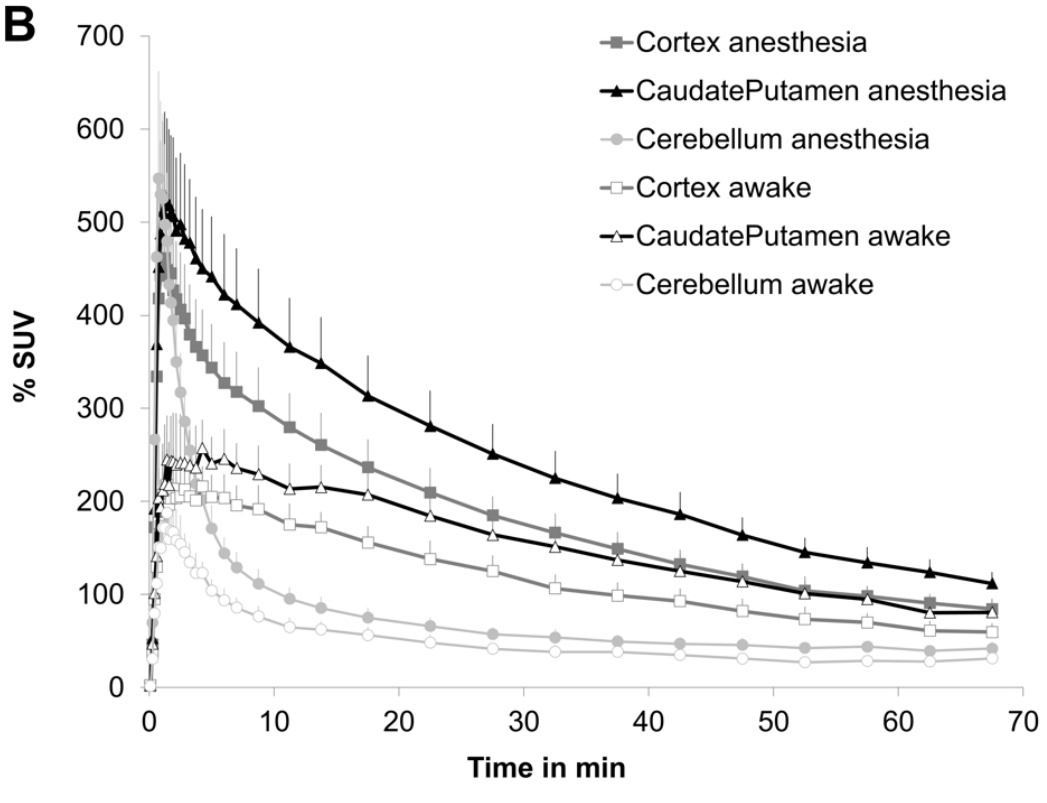
B
Cortex anesthesia
CaudatePutamen anesthesia
Cerebellum anesthesia
Cortex awake
CaudatePutamen awake
Cerebellum awake
% SUV
Time in min
0
100
200
300
400
500
600
700
0
10
20
30
40
50
60
70

Figure 3

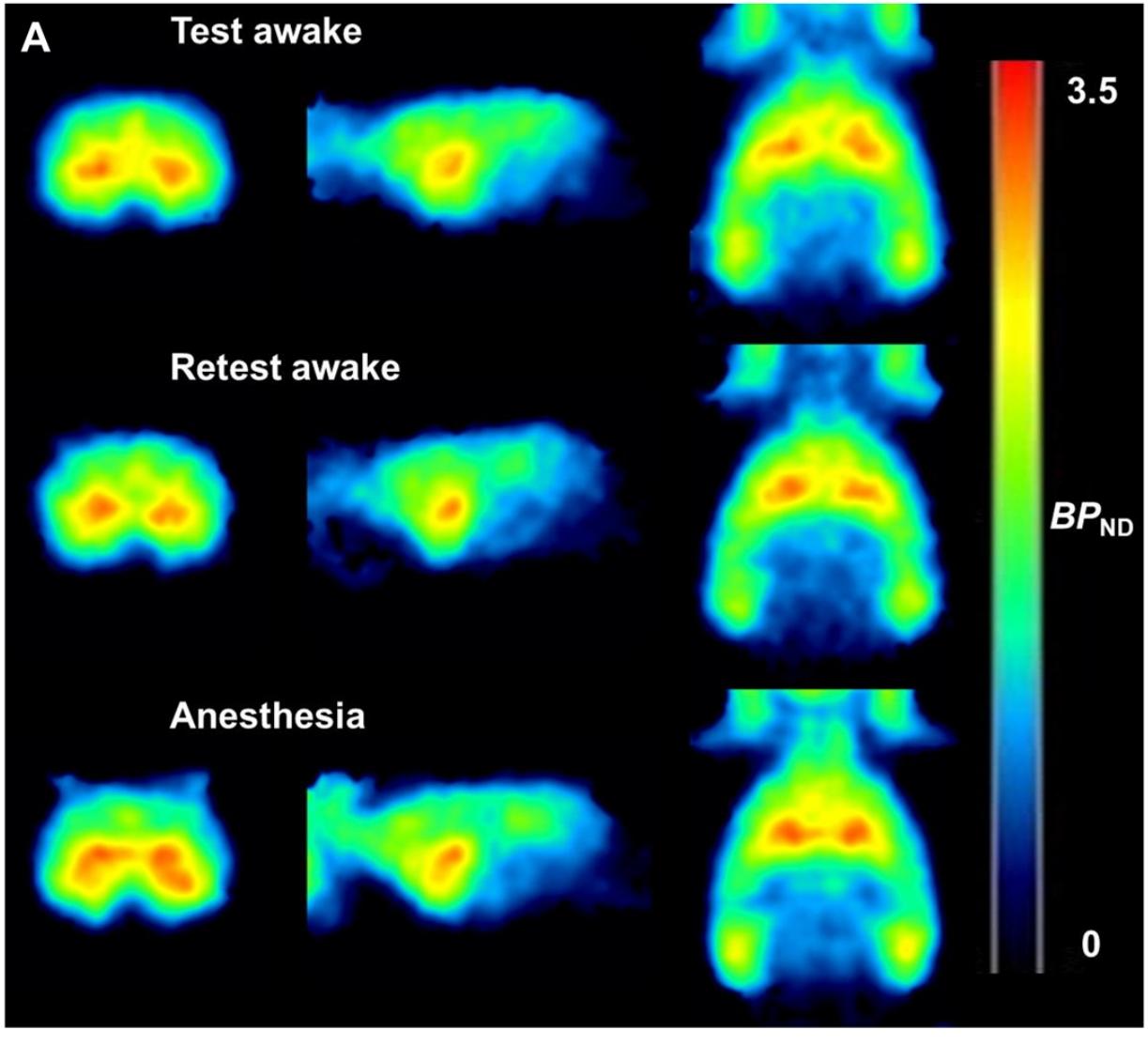
A
Test awake
Retest awake
Anesthesia
3.5
BP_{ND}
0

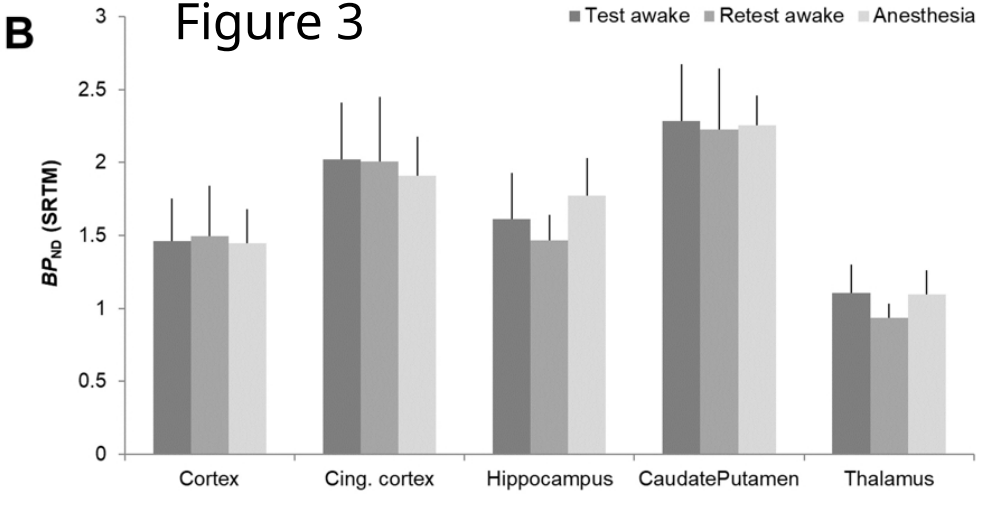
B
Test awake
Retest awake
Anesthesia
BP_{ND} (SRTM)
3
2.5
2
1.5
1
0.5
0
Cortex
Cing. cortex
Hippocampus
CaudatePutamen
Thalamus

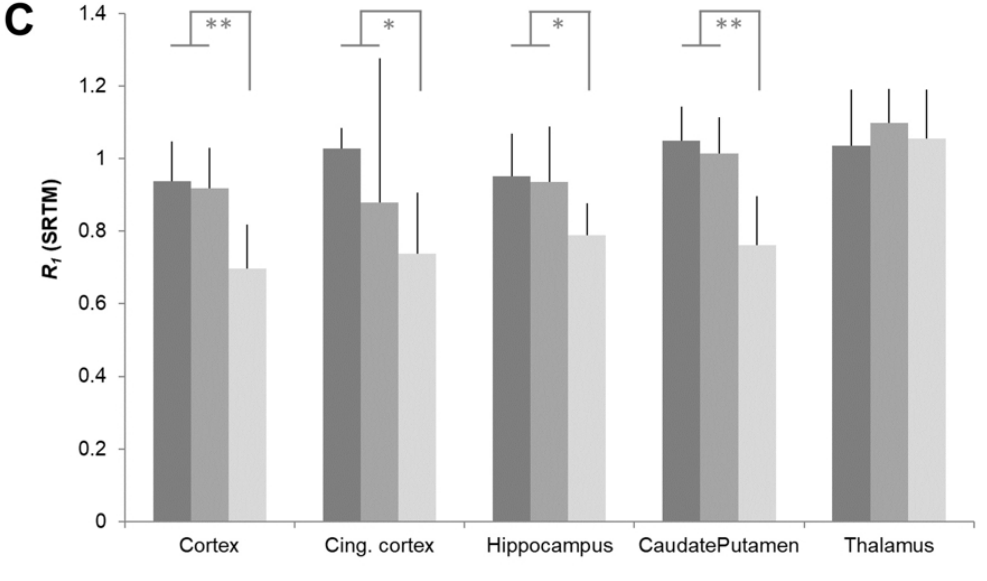
C
R_1 (SRTM)
1.4
1.2
1
0.8
0.6
0.4
0.2
0
**
*
*
**
Cortex
Cing. cortex
Hippocampus
CaudatePutamen
Thalamus

Figure 4

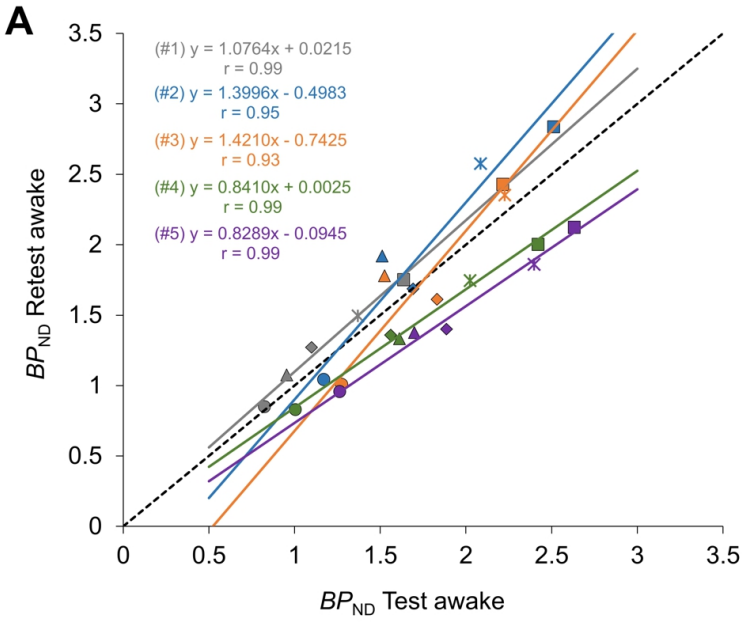
A
(#1) y = 1.0764x + 0.0215
r = 0.99
(#2) y = 1.3996x - 0.4983
r = 0.95
(#3) y = 1.4210x - 0.7425
r = 0.93
(#4) y = 0.8410x + 0.0025
r = 0.99
(#5) y = 0.8289x - 0.0945
r = 0.99
BPND Retest awake
BPND Test awake

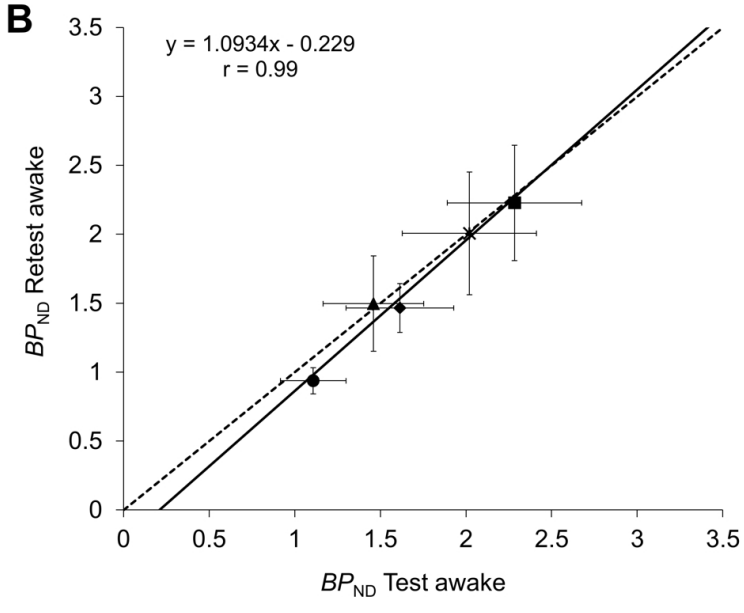
B
y = 1.0934x - 0.229
r = 0.99
BPND Retest awake
BPND Test awake

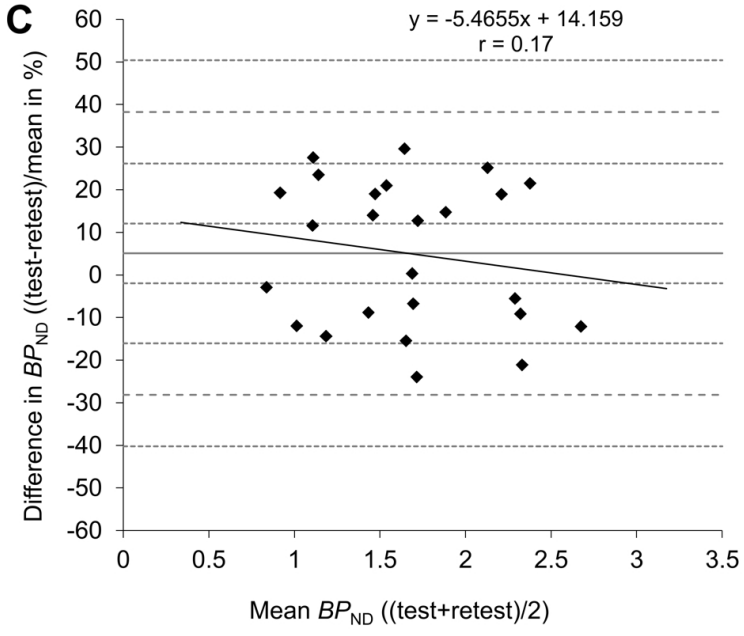
C
y = -5.4655x + 14.159
r = 0.17
Difference in BPND ((test-retest)/mean in %)
Mean BPND ((test+retest)/2)

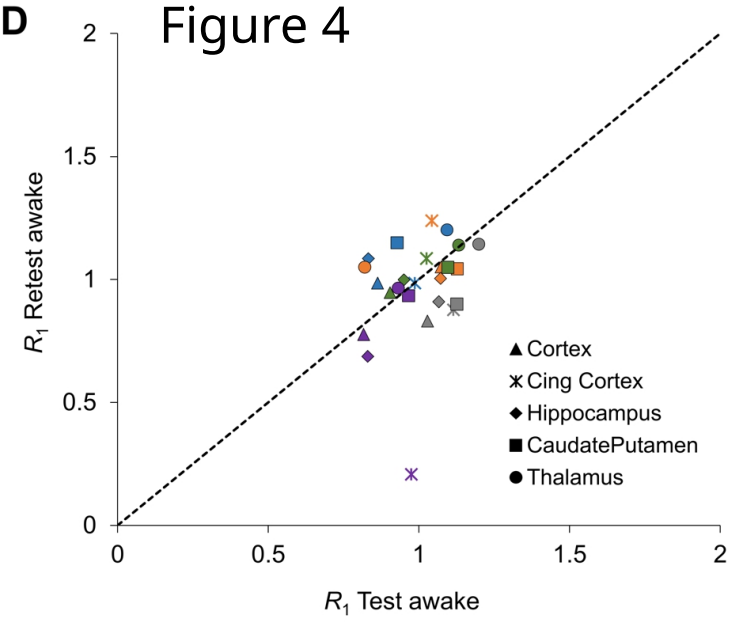
D
R1 Retest awake
R1 Test awake
Cortex
Cing Cortex
Hippocampus
CaudatePutamen
Thalamus

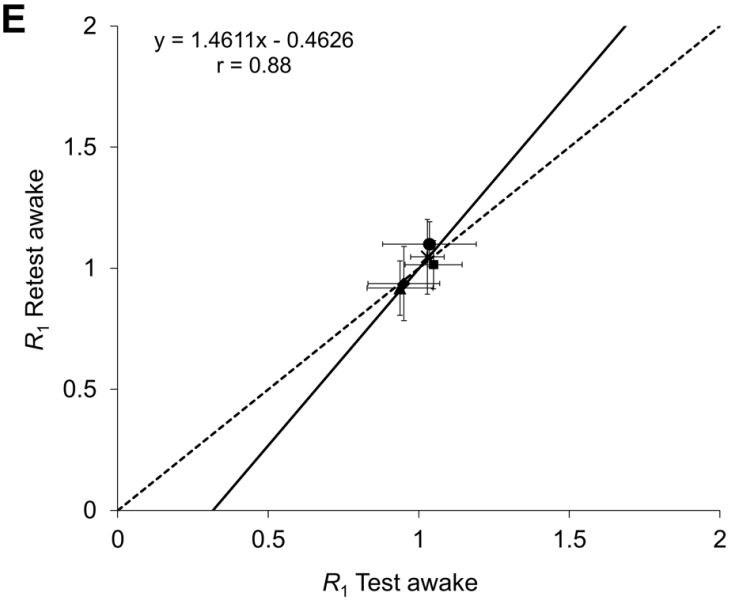
E
y = 1.4611x - 0.4626
r = 0.88
R1 Retest awake
R1 Test awake

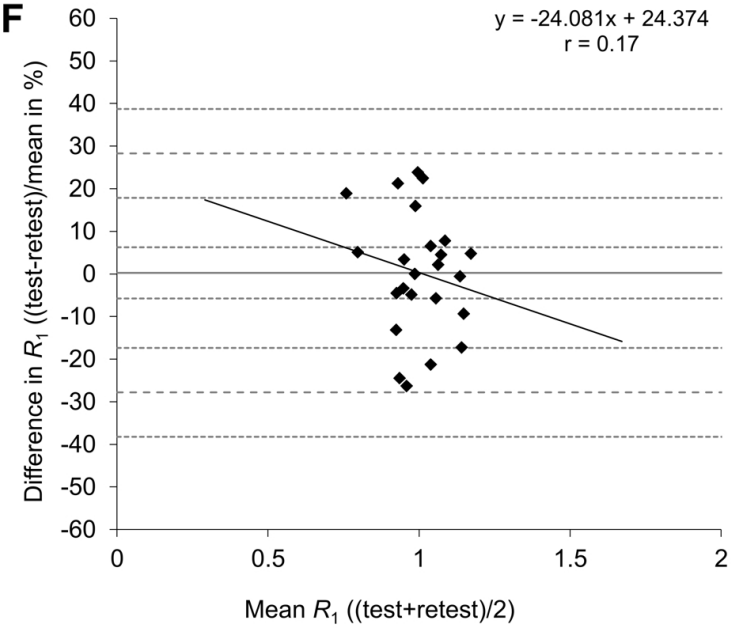
F
y = -24.081x + 24.374
r = 0.17
Difference in R1 ((test-retest)/mean in %)
Mean R1 ((test+retest)/2)

Figure 5

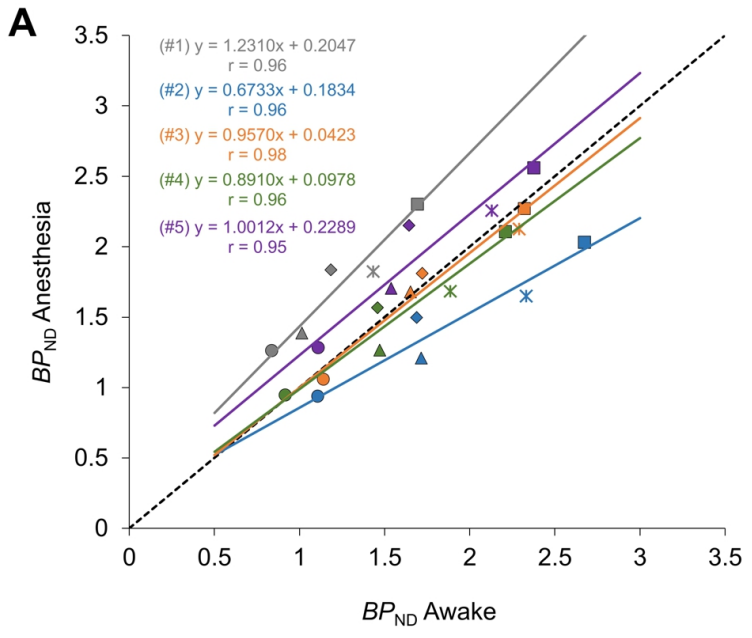
A
(#1) y = 1.2310x + 0.2047
r = 0.96
(#2) y = 0.6733x + 0.1834
r = 0.96
(#3) y = 0.9570x + 0.0423
r = 0.98
(#4) y = 0.8910x + 0.0978
r = 0.96
(#5) y = 1.0012x + 0.2289
r = 0.95
BP_ND Anesthesia
BP_ND Awake

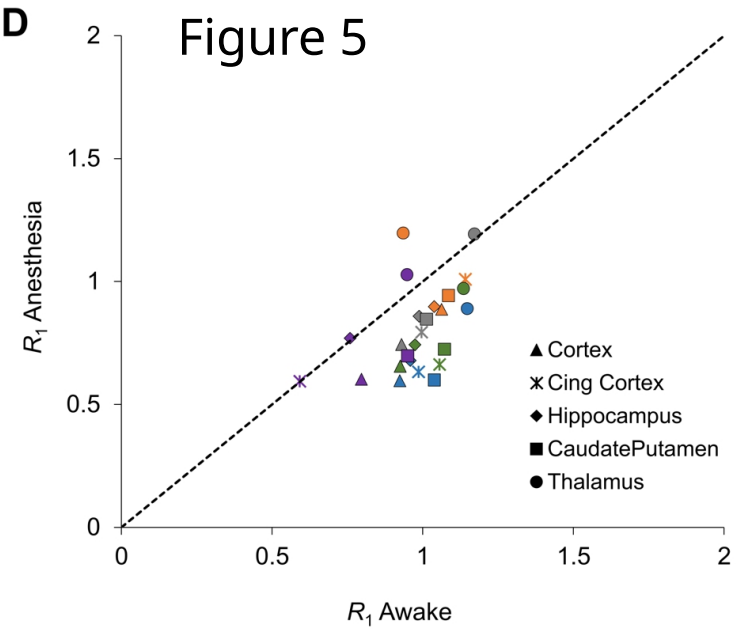
D
R1 Anesthesia
R1 Awake
Cortex
Cing Cortex
Hippocampus
CaudatePutamen
Thalamus

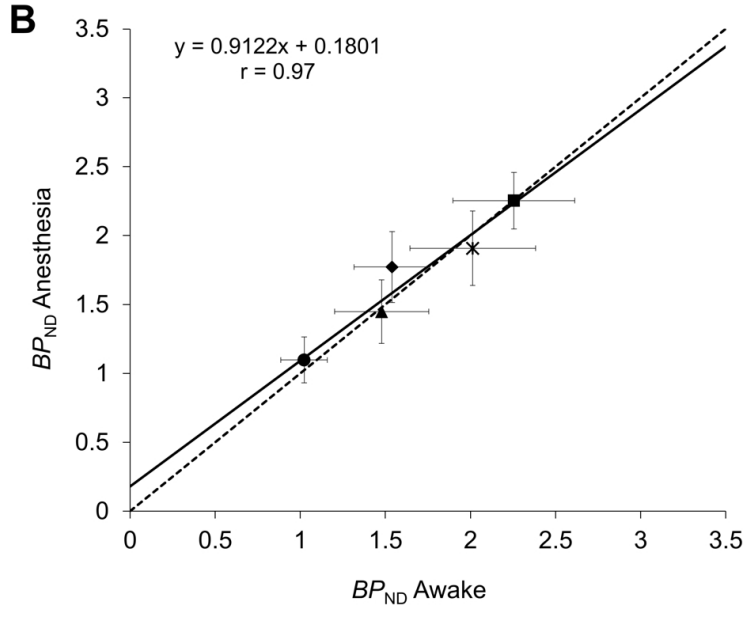
B
y = 0.9122x + 0.1801
r = 0.97
BP_ND Anesthesia
BP_ND Awake

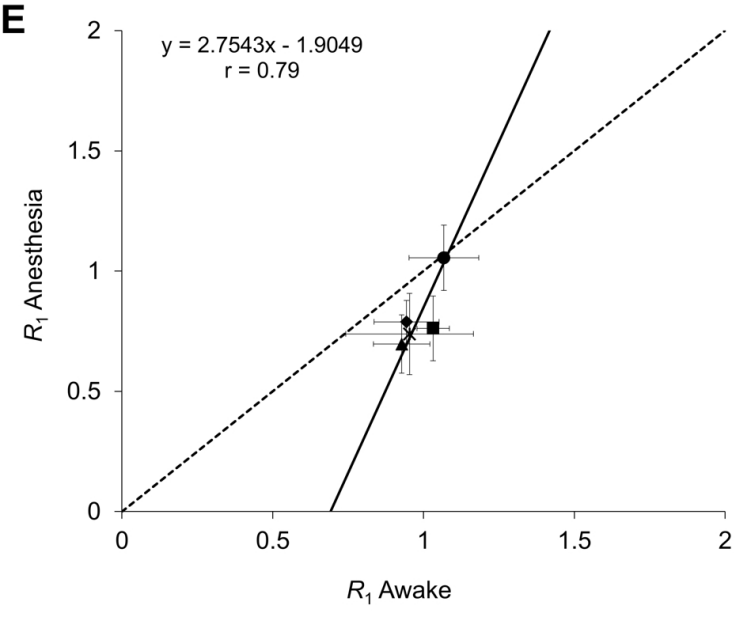
E
y = 2.7543x - 1.9049
r = 0.79
R1 Anesthesia
R1 Awake

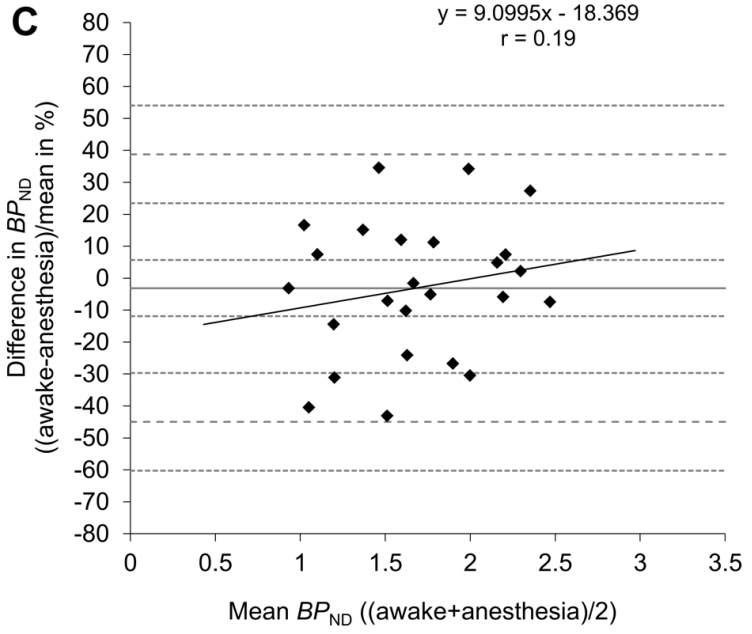
C
y = 9.0995x - 18.369
r = 0.19
Difference in BP_ND ((awake-anesthesia)/mean in %)
Mean BP_ND ((awake+anesthesia)/2)

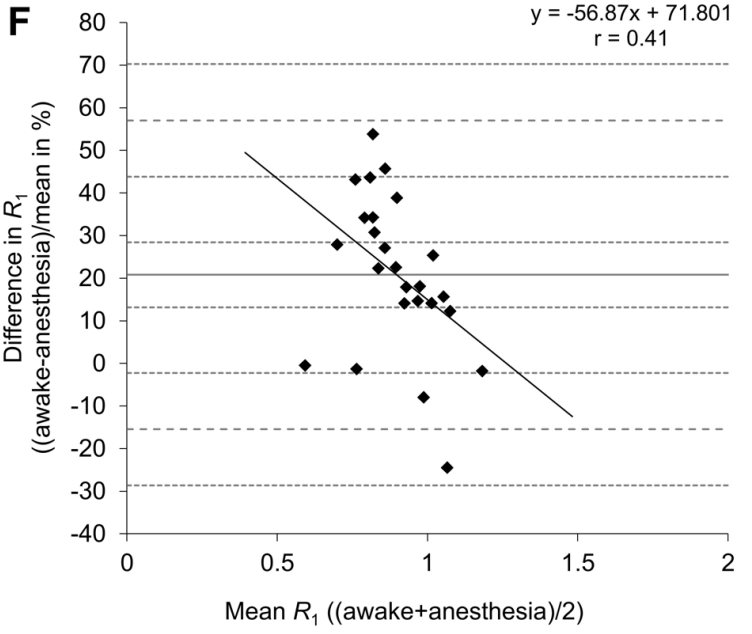
F
y = -56.87x + 71.801
r = 0.41
Difference in R1 ((awake-anesthesia)/mean in %)
Mean R1 ((awake+anesthesia)/2)